




Review Paper

Predictive calculation of structural, nonlinear optical, electronic and thermodynamic properties of andirobin molecule from ab initio and DFT methods

M. T. Ottou Abe^{1,2} · C. L. Nzia² · L. Sidjui Sidjui¹ · R. A. Yossa Kamsi² · C. D. D. Mveme⁵ · Y. Tadjouteu Assatse² · J. M. B. Ndjaka² · G. W. Ejuh^{3,4} 

Received: 20 April 2021 / Accepted: 27 July 2021

Published online: 05 August 2021

© The Author(s) 2021 **OPEN**

Abstract

The structural, nonlinear optical, electronic and thermodynamic properties of andirobin molecule were carried out by density functional theory at the B3LYP, WB97XD level and at the Restricted Hartree–Fock level by employing 6–311G(d,p) basis set. The obtained values of bond lengths, bond angles, ¹H NMR and ¹³C NMR are in good agreement with experimental values. The dipole moment and first static hyperpolarizability show that andirobin can be applied in nonlinear optical devices. HOMO–LUMO energy gap values were found to be greater than 4 eV and lead us to the conclusion that this molecule can be used as insulator in many electronic devices. The thermal energy (E), molar heat capacity at constant volume (C_v) and entropy (S) were also calculated.

Keywords Andirobin · RHF · DFT · Electronics · Nonlinear optics · Thermodynamics

1 Introduction

Currently, studies on the calculation of the electronic and physico-chemical properties of organic systems are increasingly developed [1]. The development of increasingly high-performance atomistic simulation tools has enabled researchers such as chemists and physicists to model molecular structures that can be synthesized in laboratories and that can meet the demands of the materials market. Thus, materials can be designed and produced in 2D or 3D representations with electrical properties such as electrical conductivity and HOMO–LUMO energy gap to describe their insulating, semiconducting or conducting

character. Molecules with a disordered spatial distribution can be simulated starting from a configuration corresponding to a global extremum whose energy is in the range of energies containing the local minimum or point of stability sought. More and more sophisticated modeling methods based on the solution of the Schrödinger equation such as ab-initio methods, perturbation methods and density functional theory allow to explore and obtain information from the microscopic states of materials.

Theoretical studies carried out by modeling or numerical simulations serve as a guide for experimenters by providing information that is difficult to access experimentally. In general, it is difficult to access the atomic scale

✉ G. W. Ejuh, gehwilsonjeh@yahoo.fr | ¹Laboratory of Pharmaceutical Technology, Institute of Medical Research and Medicinal Plants Studies, P.O. Box 13033, Yaoundé, Cameroon. ²Department of Physics, Faculty of Science, University of Yaoundé I, P.O. Box 812, Yaoundé, Cameroon. ³Department of General and Scientific Studies, IUT Bandjoun, University of Dschang, P.O. Box 134, Bandjoun, Cameroon. ⁴Department of Electrical and Electronic Engineering, National Higher Polytechnic Institute, University of Bamenda, P.O. Box 39, Bamili, Cameroon. ⁵Materials Science Laboratory, Department of Physics, Faculty of Science, University of Maroua, P.O. Box 814, Maroua, Cameroon.



experimentally. Modeling therefore makes it possible to obtain invaluable predictions of the properties of a molecular structure more quickly and at less cost than test methods. One of the major challenges of simulations based on quantum methods is to determine the properties of materials, including organic systems derived from medicinal plants, at the atomic scale in order to refine physical understanding and push back the limits of emerging technologies.

In Meliaceae, there are several substances whose active principle is found more in limonoids. Among them, one can find andirobin (systematic name: methyl-2-((1R,2R)-2-[(1aS, 4S, 4aS, 8aS)-4-(fluran-3-yl)-4a-methyl-8-methylene-2-oxooctahydroxireno[2,3-d]isochromen-7-yl]-2,6,6-trimethyl-5-oxocyclohex-3-en-1-yl)acetate) (Fig. 1) of molecular formula $C_{27}H_{32}O_7$ and a molar mass of 468,54 g/mol. It is a molecule with anti-inflammatory and analgesic properties, as well as anti-plasmodial activity [2, 3]. The crystal structure of andirobin [4] with the labelling of the atoms is shown in Fig. 1. This compound crystallizes in the space group $P2_12_1$ and the lattice dimensions of its orthorhombic structure are as follow: $a = 88,125 \text{ \AA}$, $b = 12,590 \text{ \AA}$, $c = 21,939 \text{ \AA}$. The Nuclear magnetic resonance (NMR) of this compound has also been reported [4, 5]. Vibrational spectroscopy and nuclear magnetic resonance (NMR) studies of active substances extracted from medicinal plants are essential to provide detailed information on their structural and vibrational properties [6–9]. However, to our knowledge, studies on this compound using Hartree Fock and DFT methods have not yet been reported in literature.

In this study, we have reported the structural, electronic, thermodynamic and nonlinear optical properties of andirobin to highlight other fields of application of this organic molecule. The paper is organized as follows. In Sect. 2, we

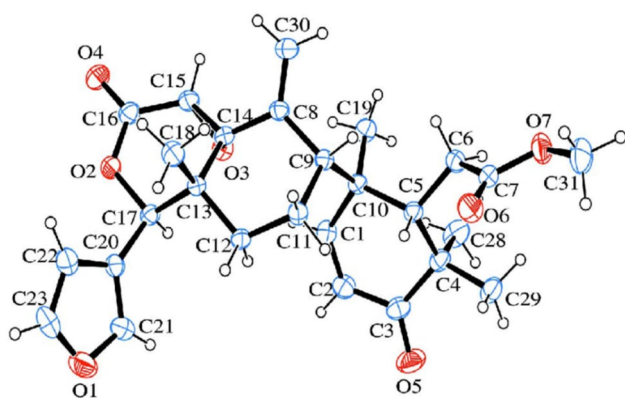


Fig. 1 The crystal structure of andirobin

describe the computational details and the theoretical framework related to this study. The results and discussions are presented in Sect. 3. The last section is the conclusion.

2 Computational details and theoretical framework

2.1 Computational details

Quantum chemical calculations were performed on andirobin using HF and DFT methods at the B3LYP and wB97XD level with the 6–311G (d,p) basis set as implemented in Gaussian 09 W software [10]. This was done in order to predict the energies, vibrational frequencies and quantum chemical properties of the studied molecular system. No geometric restriction was applied during the optimization procedure.

2.2 Theoretical framework

The calculated Raman activities (S_i) were converted into relative Raman intensities (I_i) using the relation given as follow [11]:

$$I_i = \frac{f(v_0 - v_i)^4 S_i}{v_i \left[1 - \exp\left(\frac{-hc v_i}{kT}\right) \right]} \quad (1)$$

where f is a normalization factor for all peak intensities, v_0 represents the wavenumber of the exciting laser, v_i is the wave number of the i vibrational mode, c stands for the speed of light, h and k_B are the Planck and Boltzmann constants, and T represents the temperature.

The HOMO and LUMO energies were used to determine the chemical potential, electronegativity, electrophilicity index, maximum charge transfer and chemical hardness, which are known as very important global reactivity descriptors and are calculated as follows [12]:

Chemical potential

$$\mu = \frac{E_{HOMO} + E_{LUMO}}{2} \quad (2)$$

Chemical hardness

$$\eta = (E_{HOMO} - E_{LUMO})/2 \quad (3)$$

Electronegativity

$$\chi = -(E_{HOMO} + E_{LUMO})/2 \quad (4)$$

Electrophilicity index

$$\omega = \frac{\mu^2}{2\eta} \quad (5)$$

Maximum charge transfer

$$\Delta N_{max} = -\frac{\mu}{\eta} \quad (6)$$

The optimized form of our molecule obtained using the above parameter was then used to determine NLOs properties and also by applying the formulas below which can also be found in the literature [13–15].

$$\alpha = \frac{1}{3}(\alpha_{xx} + \alpha_{yy} + \alpha_{zz}) \quad (7)$$

$$\mu = \sqrt{\mu_x^2 + \mu_y^2 + \mu_z^2} \quad (8)$$

$$\Delta\alpha = \frac{\sqrt{2}}{2} \left[(\alpha_{xx} - \alpha_{yy})^2 + (\alpha_{yy} - \alpha_{zz})^2 + (\alpha_{zz} - \alpha_{xx})^2 + 6\alpha_{xz}^2 + 6\alpha_{xy}^2 + 6\alpha_{yz}^2 \right]^{\frac{1}{2}} \quad (9)$$

$$\beta = \sqrt{(\beta_{xxx} + \beta_{xyy} + \beta_{xzz})^2 + (\beta_{yyy} + \beta_{xxy} + \beta_{yzz})^2 + (\beta_{zzz} + \beta_{xxz} + \beta_{yyz})^2} \quad (10)$$

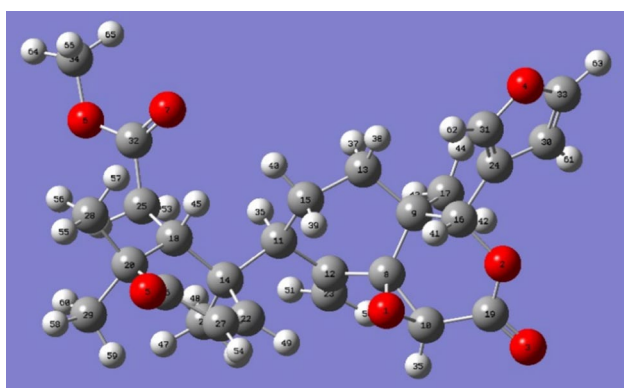


Fig. 2 The optimized structure of the andirobin molecule

3 Results and discussions

3.1 Optimized geometric structure

The optimized structure of our molecule with the adopted atomic labelling scheme is shown in Fig. 2. The total electronic energies obtained respectively using RHF, B3LYP and wB97XD with 6–311 G(d, p) are $E_{RHF} = -1565.38830231$ hartree, $E_{B3LYP} = -1575.019289$ hartree and $E_{wB97XD} = -1574.56299017$ hartree. Furthermore, no imaginary frequency was observed after optimization of our system. This led us to the conclusion that the optimized molecular systems are stable at all the levels and basis set used. From the above result we can conclude that the andirobin molecule is more stable with the functional B3LYP.

3.2 Structural properties

The optimized structural parameters such as bond lengths and bond angles of title molecule obtained using RHF, B3LYP and wB97XD level with the 6–311 G(d, p) basis set are given in the Table 1. The general analysis of all bond lengths and angles in comparison with the available experimental data is shown in Figs. 3 and 4 respectively. From Table 1, it can be observed that the calculated bond lengths and angles obtained at the level and at the basis set mentioned above are very close to the experimental

values [4]. We can also notice that these values are slightly higher than their corresponding experimental values. Furthermore, we observed that the values of bond lengths obtained at B3LYP are slightly greater than those obtained at the RHF and wB97XD level. These differences are found between 0.0044 Å and 0.0086 Å for C–O, 0.0009 Å and 0.0169 Å for C–C and 0.1154 Å and 0.1466 Å for C–H. The bond angles of the andirobin molecule are slightly different when we move from one method to another. It can be seen that the C–C–C bond angle varies from 105.1554° to 128.265°, from 105.2159° to 128.6359° and from 105.475° to 128.0052° respectively at the B3LYP, RHF and wB97XD level of theory. It can be seen in Fig. 3 that the curves for the C–O and C–C bonds coincide with each other, whereas a shift is observed for the curves of the C–H bond. This is due to the fact that the bond lengths obtained by

Table 1 Comparison between geometric, experimental and calculated parameters by B3LYP, RHF and wB97XD with 6–311 G(d,p) basis set of andirobin

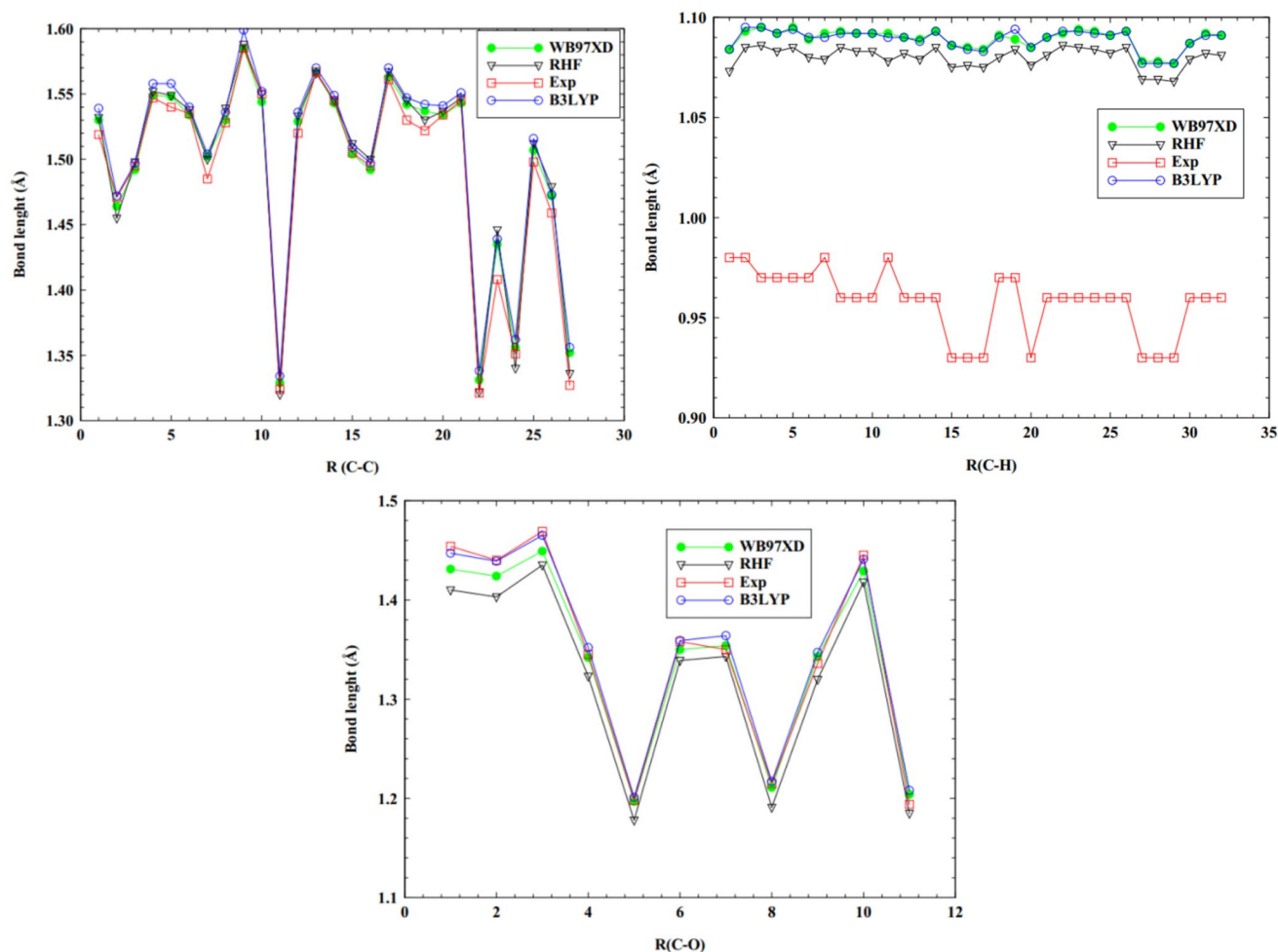
	Methods			Experimental Values [4]
	B3LYP	RHF	wB97XD	
<i>Bond lengths (Å)</i>				
(R1) O1-C8	1.44	1.41	1.43	1.45
(R2) C10-O1	1.43	1.40	1.42	1.44
(R3) O2-C16	1.46	1.44	1.45	1.47
(R4) O2-C19	1.35	1.32	1.34	1.34
(R5) C19-O3	1.20	1.18	1.20	1.20
(R6) O4-C31	1.35	1.34	1.35	1.36
(R7) O4-C33	1.36	1.34	1.35	1.35
(R8) O5-C26	1.22	1.19	1.21	1.22
(R9) O6-C32	1.35	1.32	1.34	1.34
(R10) O6-C34	1.44	1.42	1.43	1.45
(R11) O7-C32	1.21	1.19	1.20	1.19
(R12) C8-C9	1.54	1.53	1.53	1.52
(R13) C8-C10	1.47	1.45	1.46	1.47
(R14) C8-C12	1.50	1.50	1.50	1.50
(R15) C9-C13	1.56	1.55	1.55	1.55
(R16) C9-C16	1.56	1.55	1.55	1.54
(R17) C9-C17	1.54	1.54	1.53	1.54
(R18) C10-C19	1.50	1.50	1.50	1.49
(R19) C11-C12	1.54	1.54	1.53	1.53
(R20) C11-C14	1.60	1.59	1.58	1.59
(R21) C11-C15	1.55	1.55	1.54	1.55
(R22) C12-C23	1.33	1.32	1.33	1.32
(R23) C13-C15	1.53	1.53	1.53	1.52
(R24) C18-C14	1.57	1.57	1.57	1.57
(R25) C14-C21	1.55	1.55	1.54	1.55
(R26) C14-C22	1.51	1.51	1.50	1.51
(R27) C16-C24	1.50	1.50	1.49	1.50
(R28) C18-C20	1.57	1.57	1.56	1.56
(R29) C18-C25	1.55	1.55	1.54	1.53
(R30) C20-C26	1.54	1.53	1.54	1.52
(R31) C20-C28	1.54	1.54	1.53	1.53
(R32) C20-C29	1.55	1.55	1.54	1.55
(R33) C22-C27	1.34	1.32	1.33	1.32
(R34) C24-C30	1.44	1.45	1.43	1.41
(R35) C24-C31	1.36	1.34	1.36	1.35
(R36) C25-C32	1.52	1.51	1.51	1.50
(R37) C26-C27	1.47	1.48	1.47	1.46
(R38) C30-C33	1.36	1.34	1.35	1.33
<i>Bond angles (°)</i>				
(A1) C16, O2, C19	122.32	123.86	122.35	120.06
(A2) C31, O4, C33	106.75	107.08	106.87	106.10
(A3) C32, O6, C34	115.87	117.39	115.53	116.50
(A4) O1, C8, C9	115.19	115.06	115.41	115.22
(A5) O1, C8, C12	115.12	115.14	115.64	114.37
(A6) O1, C10, C19	115.22	114.36	114.99	116.20
(A7) O2, C16, C9	110.52	110.47	110.78	111.37
(A8) O2, C16, C24	105.44	105.24	105.64	105.46
(A9) O2, C19, C10	117.07	116.88	117.10	118.41

Table 1 (continued)

	Methods			Experimental Values [4]
	B3LYP	RHF	wB97XD	
(A10) O3, C19, C10	122.25	121.75	122.16	122.50
(A11) O5, C26, C20	121.84	122.32	122.22	121.80
(A12) O5, C26, C27	121.06	120.80	121.06	122.10
(A13) O4, C31, C24	110.82	111.20	110.83	110.90
(A14) O6, C32, C25	111.31	111.67	112.19	111.10
(A15) O7, C32, C25	125.36	125.03	124.74	125.40
(A16) O4, C33, C30	110.57	110.92	110.74	110.20
(A17) C9, C8, C10	117.17	117.42	116.95	116.97
(A18) C9, C8, C12	113.91	113.90	113.55	116.10
(A19) C10, C8, C12	124.38	124.39	124.70	122.08
(A20) C8, C9, C13	107.78	107.58	107.86	108.47
(A21) C8, C9, C16	106.40	106.29	106.32	107.38
(A22) C8, C9, C17	109.37	109.57	109.37	108.80
(A23) C13, C9, C16	111.88	112.18	111.82	108.19
(A24) C13, C9, C17	109.97	109.79	110.07	111.46
(A25) C16, C9, C17	111.28	111.28	111.25	112.39
(A26) C8, C10, C19	118.33	117.71	117.77	119.00
(A27) C12, C11, C14	115.56	116.04	114.76	116.50
(A28) C12, C11, C15	109.02	108.44	108.96	108.14
(A29) C14, C11, C15	113.03	113.51	113.49	115.45
(A30) C8, C12, C11	113.89	113.91	113.70	115.96
(A31) C8, C12, C23	120.40	120.25	120.47	121.50
(A32) C11, C12, C23	125.14	125.22	125.19	122.20
(A33) C9, C13, C15	114.07	114.06	113.68	113.28
(A34) C11, C14, C18	108.53	108.43	109.90	105.89
(A35) C11, C14, C21	109.61	109.99	108.85	108.42
(A36) C11, C14, C22	108.98	109.12	107.68	111.20
(A37) C18, C14, C21	112.30	112.23	111.92	113.42
(A38) C18, C14, C22	109.95	109.84	110.77	109.93
(A39) C21, C14, C22	107.43	107.19	107.58	108.03
(A40) C11, C15, C13	112.60	112.41	111.82	115.89
(A41) C9, C16, C24	116.15	116.41	114.87	115.22
(A42) C14, C18, C20	116.28	116.38	115.93	115.81
(A43) C14, C18, C25	113.21	113.01	113.05	113.03
(A44) C20, C18, C25	112.02	111.94	110.85	112.02
(A45) C18, C20, C26	109.26	108.66	109.31	105.59
(A46) C18, C20, C28	109.46	109.33	110.23	110.00
(A47) C18, C20, C29	115.93	116.49	114.76	114.23
(A48) C26, C20, C28	108.69	108.84	108.43	109.90
(A49) C26, C20, C29	105.16	105.22	105.48	105.80
(A50) C28, C20, C29	108.09	108.05	108.38	108.20
(A51) C14, C22, C27	125.60	125.91	126.08	125.40
(A52) C16, C24, C30	128.27	128.64	128.01	130.00
(A53) C16, C24, C31	126.11	126.20	126.36	125.20
(A54) C30, C24, C31	105.61	105.12	105.64	104.80
(A55) C18, C25, C32	113.52	113.91	113.06	113.70
(A56) C20, C26, C27	116.97	116.77	116.56	115.90
(A57) C22, C27, C26	123.52	123.14	122.70	123.90
(A58) C24, C30, C33	106.25	105.67	105.92	108.00

Table 1 (continued)

	Methods			Experimental Values [4]
	B3LYP	RHF	wB97XD	
(A59) O2, C19, O3	120.67	121.36	120.74	119.00
(A60) O6, C32, O7	123.29	123.24	123.06	123.40
Total energy (hartree)	-1575.019289	-1565.38830231	-1574.56299017	

**Fig. 3** Variation of the bond lengths calculated by B3LYP, wB97XD and RHF. The experimental data [4] are also illustrated for comparison

simulation are slightly greater than those obtained experimentally. Indeed, the tuning factor $\left(a_{cc} = \frac{Val_{exp} - Val_{th}}{Val_{exp}} \times 100\right)$ is between $[-15.7; 0.98]$. In Fig. 4, there is a strong coincidence of the curves for the angles C-C-H, C-C-C, C-O-C and O-C-C. On the other hand, the curves obtained for the angles H-C-H, O-C-H and O-C-O are offset from each other. This can be explained by the fact that most of the experimental values are slightly higher than those obtained by simulations. The tuning factor is included in the ranges $[0.25, 3.04]$ for H-C-H, $[0.31, 7.28]$ for O-C-H and $[-1.98, 0.85]$ for O-C-O.

Experimentally, andirobin was found to crystallize in an orthorhombic structure. After optimization of our molecular structure, we found that the bond length and bond angles are closed to the experimental results. We can therefore conclude that the optimized geometrical structure of andirobin is close to the experimental results. In this case, the lattice parameters vary slightly with optimization, and therefore, the optimized molecular structure will crystallize in the orthorhombic structure.

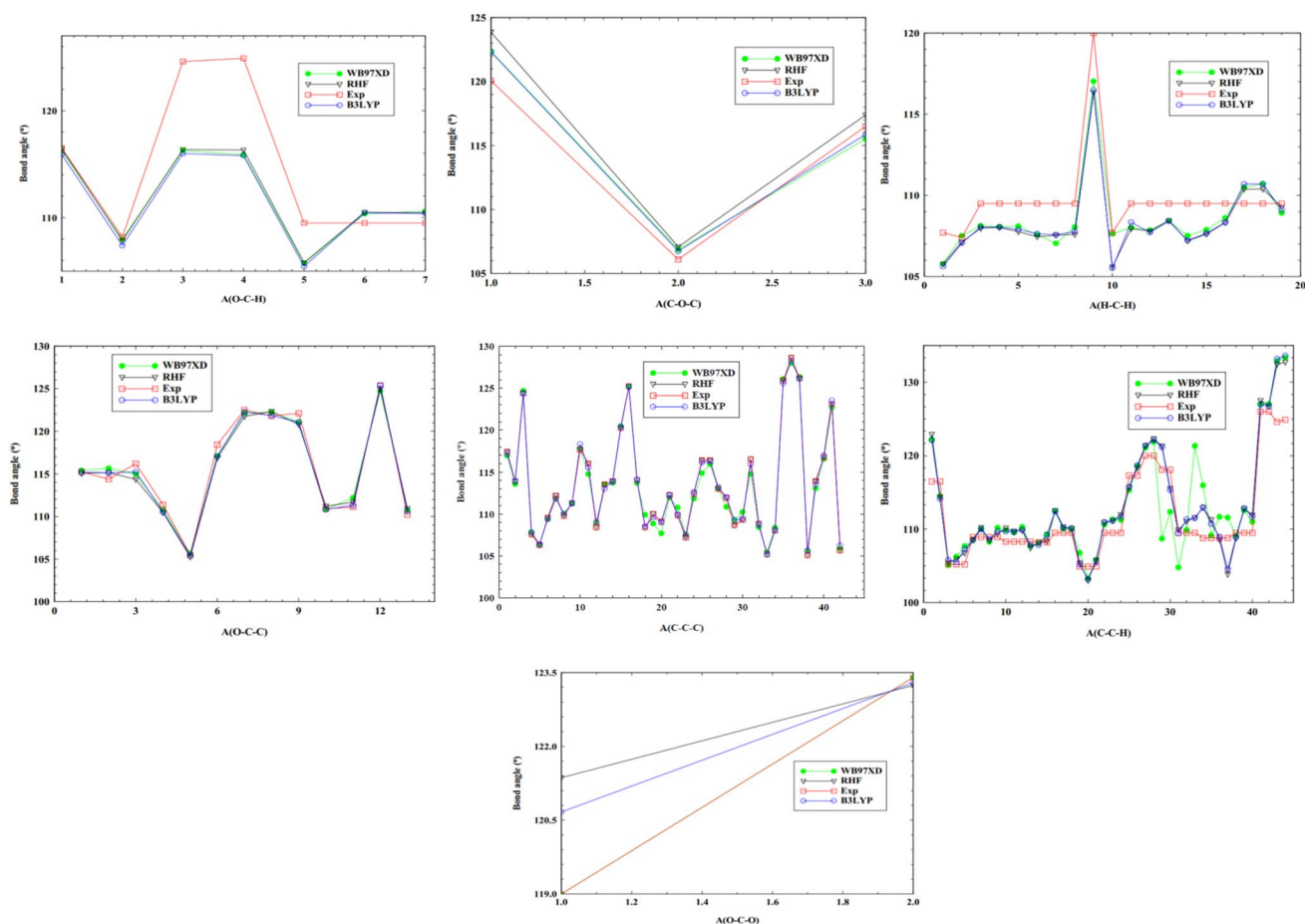


Fig. 4 Variation of the angles calculated by B3LYP, wB97XD and RHF. The experimental data [4] are also illustrated for comparison

3.3 Vibrational frequencies and assignments

Vibrational frequency analysis is a useful and important method used to estimate different movements of atoms and groups of atoms present in a molecular structure. The vibrational frequencies were calculated in this work from the optimized geometry of the title compound using RHF, B3LYP and WB97XD level with 6–311G (d,p) basis set. The experimental and computed vibrational frequencies, IR and Raman Intensities and their probable assignments with PED are presented in Table 2. The experimental and simulated vibrational spectra of andirobin are shown in Fig. 5.

The FT-IR absorption spectra (experimental Fig. 5) of andirobin [9] samples showed about eight intense absorbance bands ranging from 4000 to 500 cm^{-1} . The result showed

the stretching vibration at 1738.7 cm^{-1} and 1667.8 cm^{-1} attributed to C=O and C=C, respectively. On the other hand, the bending vibration at 1244.5 cm^{-1} is a characteristic of the C–O bonds present in the andirobin molecule. Furthermore, for the stretching vibration bands, we observed values of 2978.2 cm^{-1} , 3127.5 and 3450.0 cm^{-1} characteristic of chromophores Csp3-H, Csp2-H and O–H. While the zone corresponding to bending vibrations showed bands of mean intensity at 1030.5 cm^{-1} , 821.2 cm^{-1} and 611.4 cm^{-1} attributable to the chromophores CO (primary alcohol), C=C (vinylidene) and C=C (disubstituted alkene).

We also observed that the calculated harmonic vibrational frequencies are bigger than those obtained experimentally. Similar results have also been found by others co-workers [16, 17]. However, we observe that the IR curves of

Table 2 Comparison between infrared and Raman frequencies calculated by the RHF, B3LYP and wB97XD methods for andirobin

RHF		B3LYP		wB97XD		Intensity
Frequencies	IR	Frequencies	IR	Frequencies	IR	
3440.51	1.6372	3282.35	0.2875	3304.47	0.3632	$\mu(\text{C-H})$ furan
3421.46	1.0049	3267.41	0.3968	3290.30	0.4710	$\mu(\text{C-H})$
3412.03	0.1027	3257.63	0.0943	3281.77	0.0339	$\mu\text{sym}(\text{C-H})$
3376.28	13.7192	3221.13	11.264	3252.74	9.0315	$\mu\text{sym}(\text{CH})$
3329.34	4.3825	3177.10	7.0447	3213.71	4.7337	$\mu\text{sym}(\text{CH})$
3309.03	28.0356	3160.14	16.1540	3197.78	4.7578	$\mu(\text{C-H}) + \mu\text{sym}(\text{C-H})$
3295.72	6.5214	3140.08	5.2622	3195.15	2.6611	$\mu\text{asym}(\text{C-H})$
3284.90	28.2614	3124.52	19.0971	3189.40	11.8999	$\mu\text{sym}(\text{C-H})$
3272.72	11.8533	3089.31	11.8867	3170.96	6.6206	$\mu(\text{C-H})$
3258.83	30.1146	3113.15	17.3067	3164.93	7.8378	$\mu\text{sym}(\text{C-H})$
3235.76	19.9841	3096.67	16.5451	3164.37	4.5421	$\mu\text{sym}(\text{C-H})$
3186.15	23.0332	3041.79	12.6074	3150.05	14.0794	$\mu\text{sym}(\text{C-H})$
3183.37	19.3625	3039.03	15.2018	3148.46	25.7896	$\mu\text{sym}(\text{C-H})$
3174.73	26.4816	3033.97	22.2810	3145.85	12.1334	$\mu\text{sym}(\text{C-H})$
2021.02	628.6489	1823.77	438.8536	1809.58	280.8891	$\mu(\text{O-C}) + \delta(\text{O-C-C}) + \delta(\text{H-C-C})$
1972.90	266.1451	1791.26	186.7560	1737.24	6.7040	$\mu(\text{O-C}) + \delta(\text{H-C-C})$
1964.12	383.3138	1747.67	257.0083	1732.49	12.6819	$\mu(\text{C-O}) + \delta(\text{H-C-C})$
1849.15	5.4678	1694.33	8.4959	1670.17	4.6104	$\delta(\text{H-C-H}) + \mu(\text{C-C})$
1838.11	11.0471	1680.56	17.4432	1567.17	28.3066	$\delta(\text{C-C-H}) + \mu(\text{C-C})$
1792.86	6.3720	1626.02	3.3831	1498.69	15.0107	$\mu(\text{C-C}) + \delta(\text{O-C-H})$
1688.90	42.3500	1533.81	25.7481	1495.08	14.5884	$\mu(\text{C-C}) + \delta(\text{O-C-H})$
1633.28	12.4096	1512.91	11.6690	1451.63	9.1101	$\delta(\text{C-H})$
1624.42	3.6765	1526.39	10.7939	1442.87	27.3968	$\delta(\text{C-H})$
1612.68	44.2483	1472.15	17.4611	1424.65	17.2955	$\delta(\text{C-H})$

μ : stretching, μsym : symmetric stretching, μasym : asymmetric stretching, δ : Flexion

the RHF, B3LYP and wB97XD methods with the 6–311 G(d,p) basis set are slightly offset from each other. This difference is mainly due to the fact that the RHF does not take into account the electronic correlation unlike the B3LYP and wB97XD.

3.4 Vibrational study of functional groups

3.4.1 C–H Vibration

In literature, it is known that C–H stretching vibrations in alkanes and aromatic structures are located in the regions of 2850–3000 cm^{-1} and 3000–3100 cm^{-1} , respectively [18]. From Fig. 5, the FT-IR bands for C–H stretching vibrations are observed at 2978 cm^{-1} . This value is in agreement with experimental data in the literature [19, 20]. Using the Hartree–Fock and DFT methods, we observed CH stretching vibrations at 3050.51–2912.7 cm^{-1} , while the in-plane and out-of-plane bending vibrations involving

CH bonding were observed between 1049 and 988 cm^{-1} and 775–593 cm^{-1} .

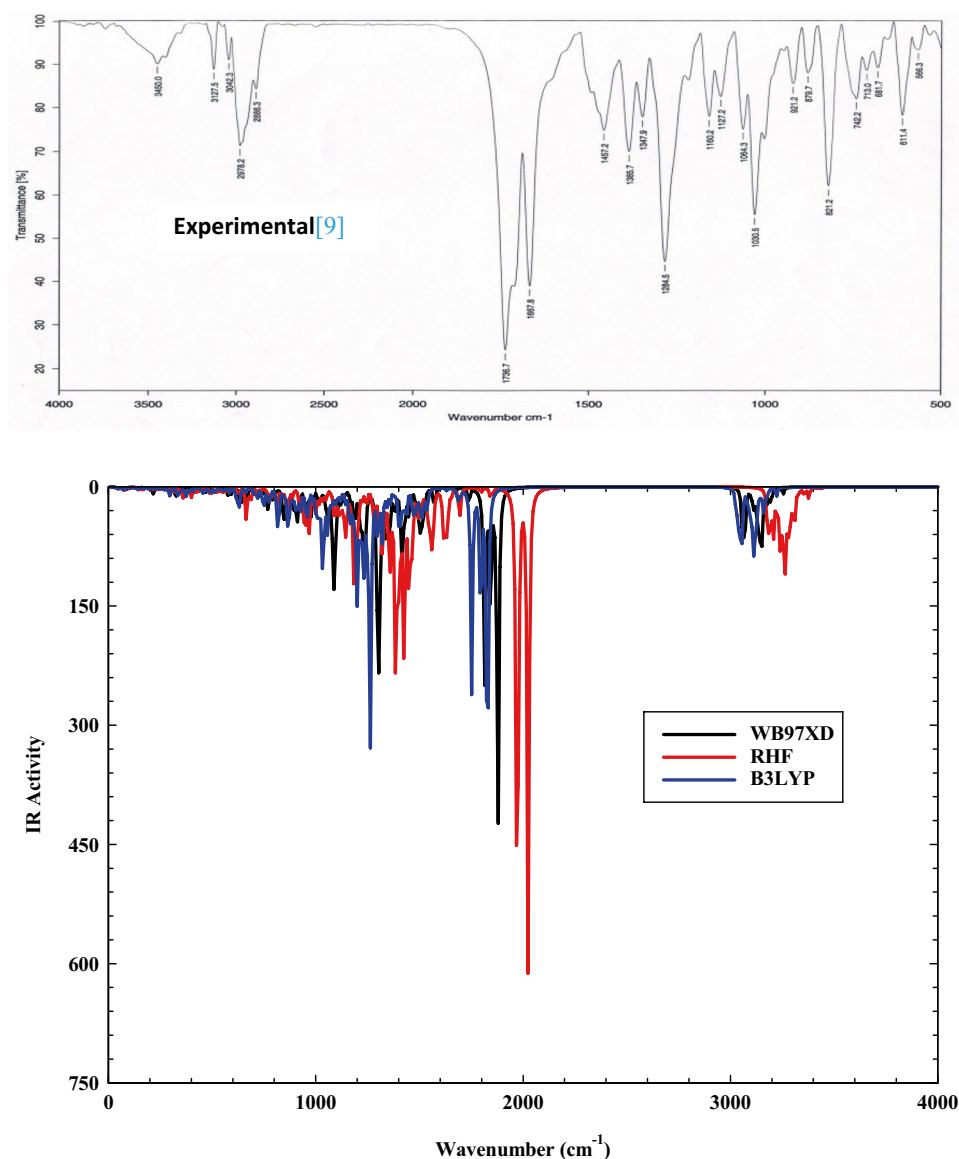
3.4.2 C=O Vibration

The C=O bond in the ester gives rise to characteristic bands in the IR spectrum covering the spectral range from 1730 to 1750 cm^{-1} [20]. In the andirobin molecule, we observe a C=O stretching vibration in the frequency range 1838–2021 cm^{-1} in good agreement with the experimental data. In-plane and out-of-plane bending vibrations are observed in the frequency ranges 1545–533 cm^{-1} and 1463–859 cm^{-1} for infrared spectra.

3.5 NMR Study

The GIAO (Gauge Invariant Atomic Orbitals) method [21–23] was used to predict the ^1H and ^{13}C chemical shifts at the RHF, B3LYP and wB97XD levels with the 6–311 G (d, p) basis set.

Fig. 5 Experimental data [9] and calculated infrared spectra of andirobin with B3LYP, wB97XD and RHF methods



The TMS (Tetramethylsilane) was used to convert chemical shielding to chemical shift. The following equation was used for this purpose:

$$\delta_i(\text{ppm}) = \text{isotropic}(TMS_i) - \text{isotropic}(i) \quad (11)$$

where i is the atom type. The experimental and calculated values of ^{13}C and ^1H chemical shift are presented in Tables 3 and 4. The positions of the atoms were numbered as in Fig. 1. From Table 3, it can be observed that RHF provides results of ^{13}C chemical shift, which are very close to the experimental values than those obtained using B3LYP and wB97XD with the exception of the carbon atoms directly linked to the oxygen atoms. The same observation

is made for the ^1H chemical shift as shown in Table 4. For more clarity, we show the experimental ^{13}C NMR and ^1H NMR spectra of andirobin obtained by Sidjui et al. [9] and represented respectively in Figs. 6 and 7. The experiment and calculations were carried out in a chloroform solvent. The comparison between the experimental and theoretical calculations is shown in Figs. 1 and 2 for the ^{13}C and ^1H NMR respectively.

The following figures show the comparison between the experimental [9] and calculated values of ^{13}C and ^1H chemical shift. The regression line was plotted for each method using the equation $\delta_{cal} = a\delta_{exp} + b$, where a and b are given in Figs. 8 and 9. The values of r^2 show that our

Table 3 Experimental [9] and calculated ^{13}C NMR chemical shift δ (ppm) of andirobin at the RHF, B3LYP and wB97XD method with 6–311 G(d,p) basis set

Nuclei	Calculated δ (ppm)			Experiment δ (ppm)
	RHF	wB97XD	B3LYP	
C8	58.825275	72.1877	77.4143	67.8
C9	35.220875	43.6673	47.3966	38.6
C10	48.459275	58.0134	61.0948	77.4
C11	43.219275	54.0043	56.499	48.8
C12	148.589175	153.7904	155.6258	138.9
C13	28.492975	34.6573	36.6703	29.5
C14	38.627775	47.7159	52.7752	43.1
C15	19.874875	24.9355	27.0265	21.3
C16	67.287475	77.4367	81.8547	55.5
C17	19.404175	22.5538	22.9991	14.6
C18	36.839375	48.3799	50.4954	42.8
C19	165.438075	169.7997	171.3369	166.7
C20	41.433675	49.9498	53.6616	46.1
C21	19.957375	24.0433	23.4051	20.2
C22	159.709075	162.858	164.2847	153.5
C23	126.978075	129.177	127.7691	122.3
C24	126.053975	129.7618	131.3856	119.8
C25	30.256375	35.653	36.2744	31.5
C26	199.269975	205.4942	207.5041	203.7
C27	129.626675	133.9158	135.3459	125.7
C28	22.543375	26.6395	26.4744	22.7
C29	21.179575	26.1283	25.8516	22.5
C30	115.380475	117.7129	118.6176	109.7
C31	145.054675	146.2504	148.1928	140.9
C32	177.144775	181.8408	184.2684	174.3
C33	146.749175	149.2961	150.6662	143.2

results are close to experimental results. The linear correlation coefficient calculated as *R*-square found in Figs. 8 and 9 also confirms this.

3.6 Electronic properties

3.6.1 Frontier molecular orbitals

The molecular mechanism of the reactivity of the molecule can be described by the frontier molecular orbitals; these are two particular types of molecular orbitals: HOMO (Highest Occupied Molecular Orbital) and LUMO (Lowest Unoccupied Molecular Orbital) [24]. The HOMO–LUMO energy gap and the global reactivity descriptors of the

Table 4 Experimental [9] and calculated ^1H NMR chemical shift δ (ppm) of andirobin at the RHF, B3LYP and wB97XD method with 6–311 G(d,p) basis set

Nuclei	Calculated δ (ppm)			Experiment δ (ppm)
	RHF	wB97XD	B3LYP	
H35	3.13935	3.6019	3.6937	3.97
H36	2.04655	2.2351	2.6963	2.39
H37	0.56755	0.7542	1.0249	1.60
H38	1.37525	1.7454	1.9293	1.16
H39	1.30255	1.5244	1.7389	1.90
H40	1.95615	2.0312	2.6714	1.73
H41	4.94455	5.6571	5.8662	5.41
H45	2.22555	2.6919	3.0549	2.62
H49	6.93735	7.1027	7.4193	7.07
H50	5.56125	5.862	5.8088	5.30
H51	5.41655	5.8363	5.6708	5.2
H52	2.00905	2.5359	2.6614	2.44
H53	1.72775	2.6979	2.3135	2.28
H54	6.08425	2.4126	6.3678	5.99
H61	6.60765	6.9032	6.8907	6.27
H62	7.33725	7.5707	7.6155	7.33
H63	7.39645	7.6535	7.7025	7.34

molecule are given in Table 5. The values of these parameters were determined using B3LYP, wB97XD and RHF methods with the 6–311 G(d,p) basis set. Figure 10 shows the atomic compositions of the frontier molecular orbitals. In this Fig. 10, the red color stands for surfaces of high electron density and the green color stands for surfaces of low electron density. From the data obtained using the three methods, we find that the HOMO binds to the furan group while the LUMO is located on a ring comprising the C=O and C=C bonds which means that the electron transfer would take place from the furan group to the C=O and C=C groups. The energy gap of the andirobin (5.06 eV) obtained by B3LYP is lower than that obtained using RHF (11.89 eV) and wB97XD (9.11 eV) methods with 6–311 G(d, p) basis set. In addition, from Table 5, we observe that η decreases from the RHF method to the wB97XD and B3LYP method which means that the molecule is more reactive with the B3LYP. This can also be confirmed by a decrease in the energy gap and an increase in softness as well as by the value of the electrophilicity index which increases. The gap being greater than 4 eV, it can be concluded that andirobin can be used as an insulator for the design of electronic devices.

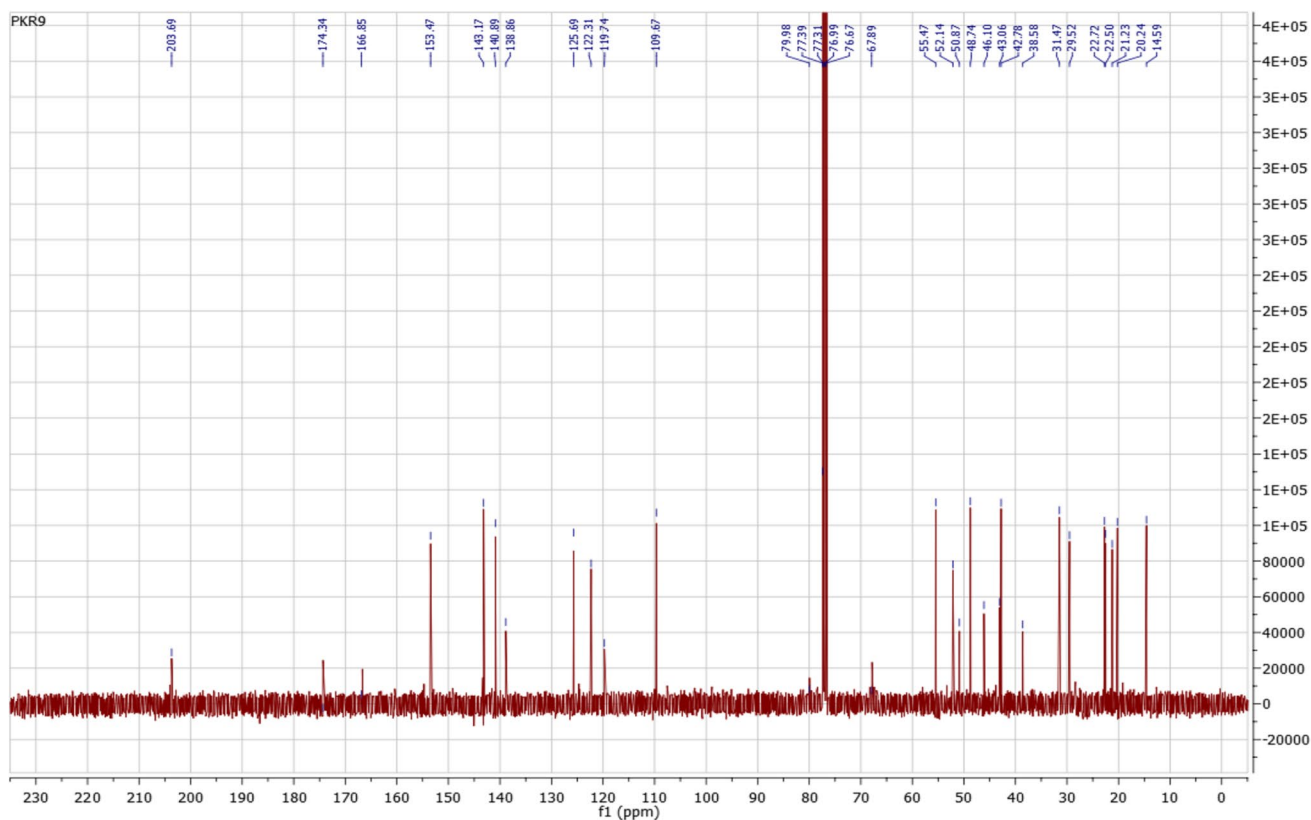


Fig. 6 Experimental data ^{13}C NMR spectrum of andirobin (CDCl_3) [9]

3.6.2 Atomic charge analysis of andirobin

The atomic charge analysis plays an important role in the study of molecular systems because atomic charges have an effect on dipole moment, molecular polarizability, electronic structure and many other molecular properties of the system [24]. It also makes it possible to predict the types of bonds that may [25] be formed.

The natural atomic charge values calculated from the Mulliken population analysis of andirobin using the DFT and HF methods are illustrated in Fig. 11.

We notice that all the hydrogen and oxygen atoms have a positive charge and a negative charge, respectively. On the other hand, the carbon atoms do not all have the same sign charge; this is due to the presence of C–H and C–O bonds. The presence of these different signs of the charge makes it possible the formation of intramolecular and intermolecular interactions through the C–H, C=C, C=O and O–H bonds which are the different functional groups of the molecule.

3.7 Thermodynamic properties

Thermodynamics parameters of andirobin were calculated using B3LYP, wB97XD and RHF methods with 6–311 G(d,p) basis set and are listed in Table 6. The total energy of a molecule is the sum of the translational, rotational, vibrational and electronic energies:

$$E = E_t + E_r + E_v + E_e \quad (12)$$

The difference between the values calculated by two methods is marginal. Relationships between partition functions and various thermodynamic functions have been used to evaluate the partition function due to the degrees of freedom of translation, rotation and vibration of the movements of the molecule [25]. The thermodynamic parameters such as energy (E), Molar heat capacity at constant volume (C_v) and entropy (S) were calculated for andirobin at room temperature using RHF, B3LYP and wB97XD methods. The calculated values can be found in Table 6. We observed from this table that the total energy

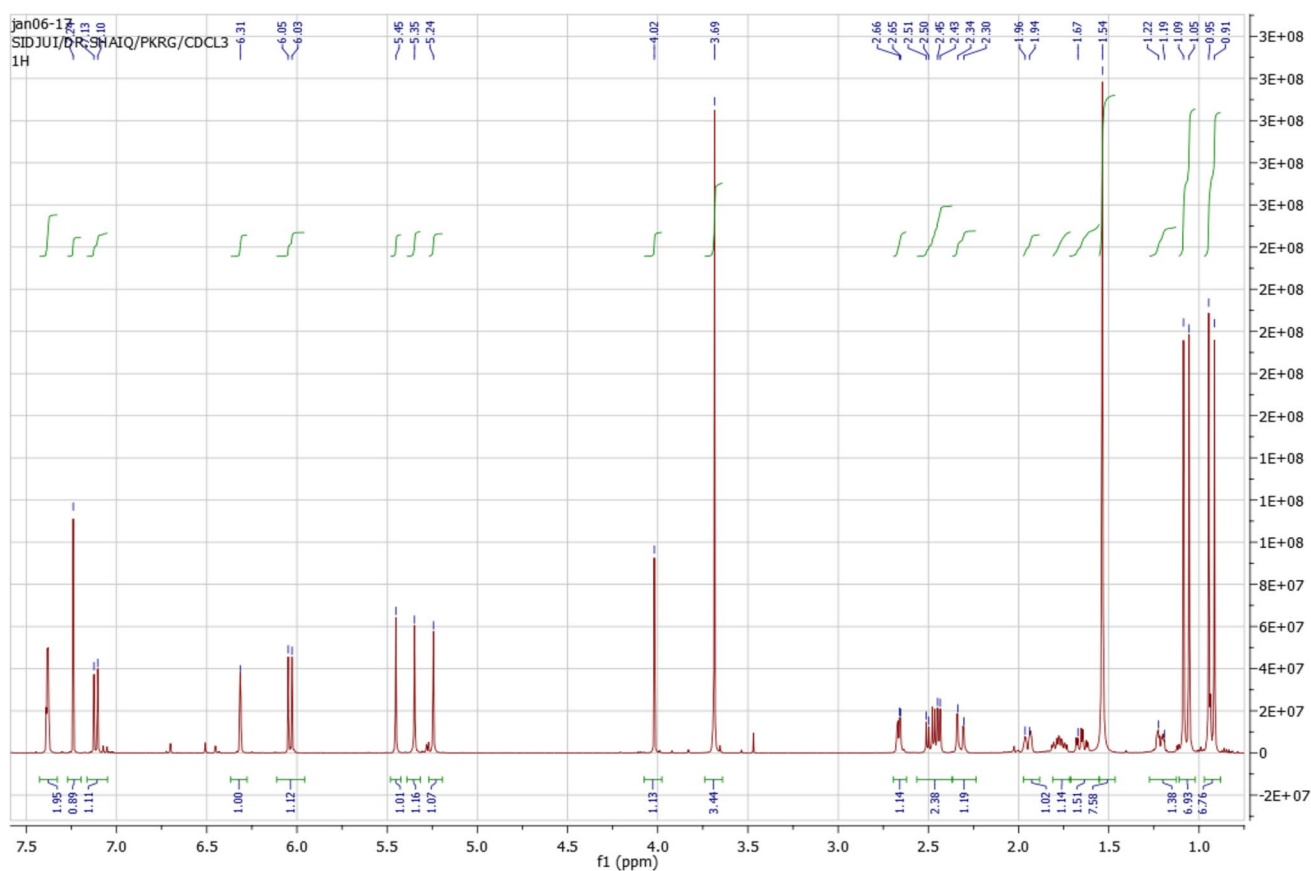


Fig. 7 Experimental data ^1H NMR spectrum of andirobin (CDCl_3) [9]

(E) of the molecule decreases slightly when we move from the RHF to wB97XD and B3LYP. We also found that the heat capacity at constant volume (C_v) and the entropy (S) are higher at the B3LYP/6-311G (d,p) level. This can be explained by the fact that the vibrational part of these parameters are higher with B3LYP. To our knowledge, no thermodynamic property had yet been studied on the andirobin molecule to compare our results.

3.8 Non-linear optical properties

Materials with appropriate nonlinear responses to incident light can be exploited to modify propagation characteristics such as the frequency, amplitude or phase of transmitted electromagnetic radiation. These materials make it possible to adapt the nature of light to particular applications [26, 27]. Currently, many studies are being done on the determination of the non-linear optical properties of organic molecules. Indeed, organ systems generally have

excellent electrical response properties such as hyperpolarizability and polarizability at the microscopic level. The large values of the non-linear responses may be due to the very rapid response or relaxation time of the material, as well as to the movement of π electrons in electronic clouds between the donor and acceptor groups. In this context, some parameters of nonlinear optical properties (NLO) such as dipole moment (μ), mean polarizability (α_0), anisotropy ($\Delta\alpha$), first order hyperpolarizability (β_0) were calculated in this work with the RHF, B3LYP and wB97XD level using 6–311 G(d,p) basis set by applying the relations (7–10) mentioned above. Table 7 shows these values. We observe that α_0 , $\Delta\alpha$ and β_0 increase when we move from RHF to wB97XD and from wB97XD to B3LYP. It is also noted that these values increase as the energy gap decreases. We can therefore conclude that the increase of these values (α_0 , $\Delta\alpha$ and β_0) improves the reactivity of our system. This can be explained by the strong dynamics of charge carriers within these structures. The large α_0 values of andirobin

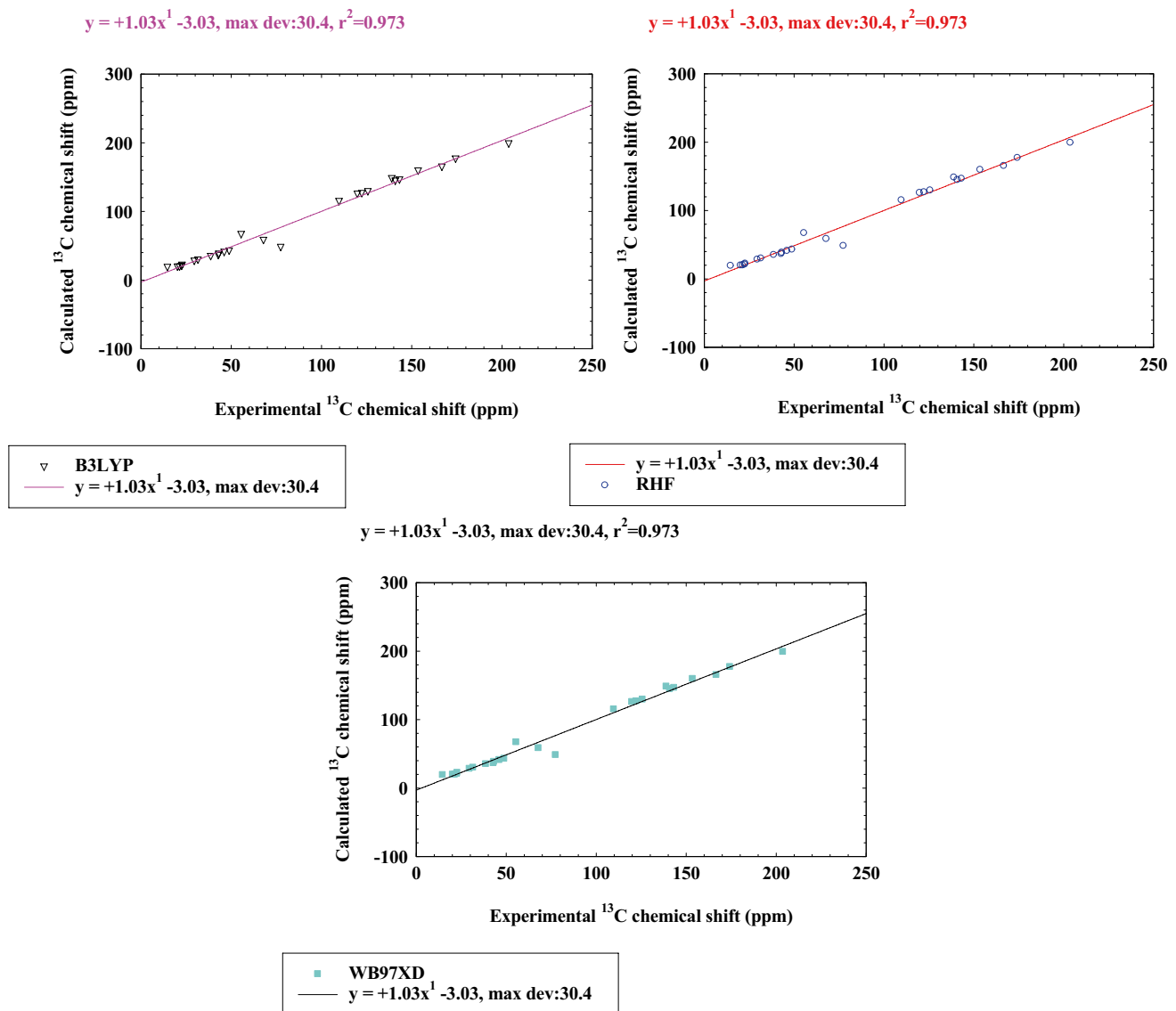


Fig. 8 Comparison of experimental [9] and theoretical ^{13}C chemical shifts of andirobin calculated at the RHF, B3LYP and wb97XD levels with 6–311 G(d,p) basis set

with B3LYP suggest that the interaction of light or other electromagnetic fields polarizes the charge distribution and modifies the propagated field. The calculated values of polarizability (α_0) and first static hyperpolarizability (β_0) obtained from Gaussian output are in atomic units. These values were then converted into electrostatic unit (esu) for comparison (for α_0 : 1 a.u. = 0.1482×10^{-24} esu, for β_0 : 1 a.u. = 8.6393×10^{-33} esu) [17]. For a given molecule, when these values (μ and β) are greater than those of urea ($\mu = 3.8851 \text{ D}$ and $\beta_0 = 372.8 \times 10^{-33}$ esu) [17, 28, 29], the

molecule has good active NLO properties. Similarly when we compare the values of μ and β_0 of andirobin with the experimental values of urea, our values are much higher than those of urea. We can conclude that, in addition to its insulating character, the andirobin molecule can also have applications in the field of nonlinear optics, especially in the development of many technologies such as optical information processing, telecommunications, integrated optics, optical computers and laser technology [14, 30–32].

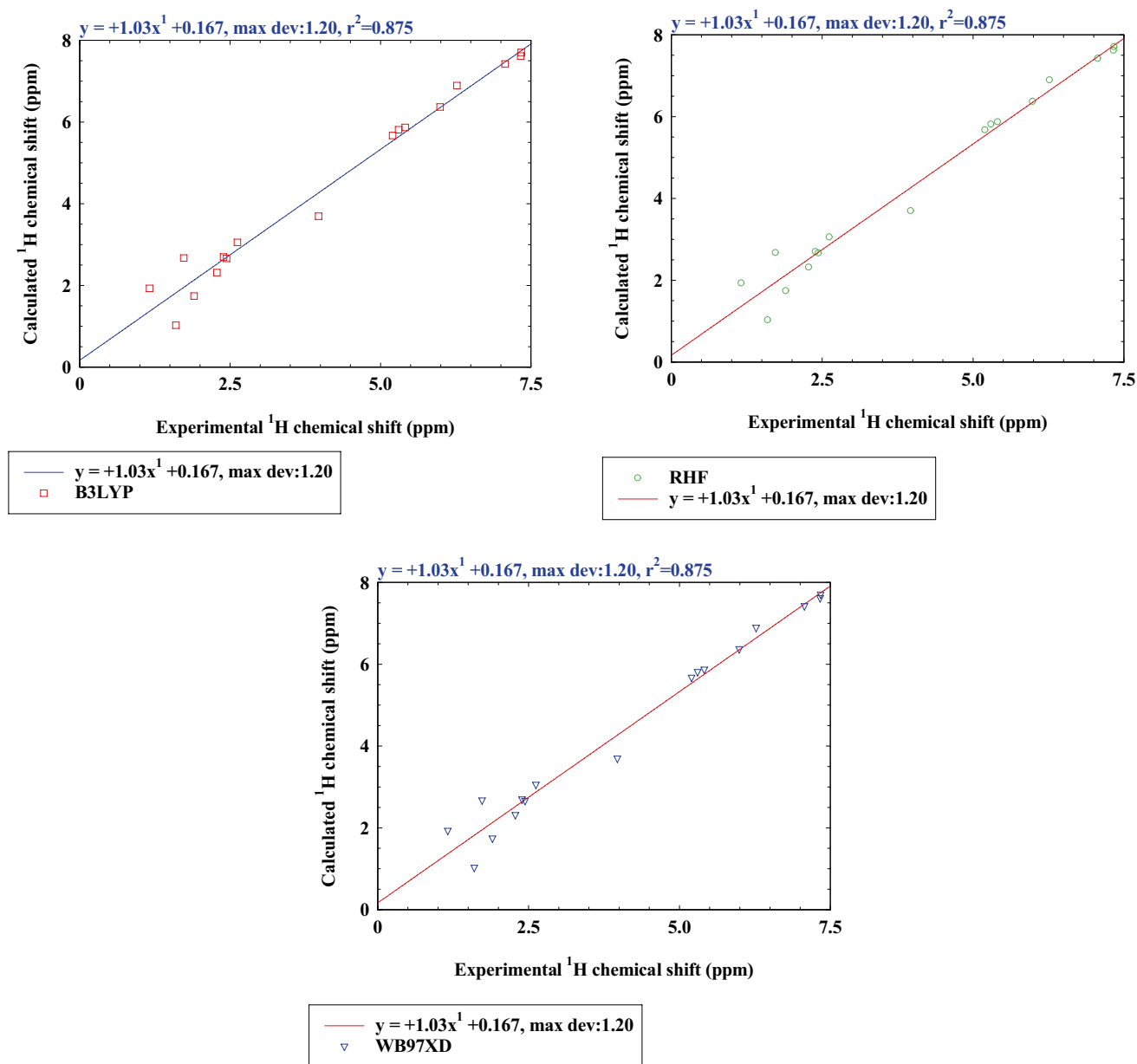


Fig. 9 Comparison of experimental [9] and theoretical ^1H chemical shifts of andirobin calculated at the RHF, B3LYP and wB97XD levels with 6–311 G(d,p) basis set

Table 5 Overall reactivity indices of andirobin obtained by RHF, wB97XD and B3LYP methods with 6–311 G(d,p) basis set

Molecular properties	RHF	wB97XD	B3LYP
E_{HOMO} (eV)	-9.01	-8.68	-6.63
E_{LUMO} (eV)	2.89	0.43	-1.57
Gap energy E_{gap} (eV)	11.89	9.11	5.062
Ionization potential (I) (eV)	9.01	8.68	6.63
Electron affinity (A) (eV)	-2.89	-0.43	1.57
Chemical potential (μ)	-3.06	-4.12	-4.10
Absolute hardness (η)	5.95	4.56	2.53
Electronegativity (χ)	3.06	4.12	4.10
Electrophilicity (ω)	0.79	1.87	3.32
Maximum charge transfer (ΔN_{max})	0.51	0.91	1.62

4 Conclusion

This study has allowed us to characterize the structural, nonlinear optical, electronic and thermodynamic properties of andirobin. We have found that with regard to the structural properties, the parameters of the optimized geometrical structure (bond lengths and bond angles) obtained by numerical computations correspond correctly to those found experimentally. A good agreement with the experiment was also found for ^1H NMR and ^{13}C NMR. Concerning the electronic properties obtained, andirobin is an insulator because its energy gap is greater than 4 eV. Moreover, the nonlinear optical properties reveal that andirobin is a polar molecule ($\mu \neq 0$). Similarly, the value of the first order hyperpolarizability is higher than that of urea, which allowed us to say that andirobin is a molecule that

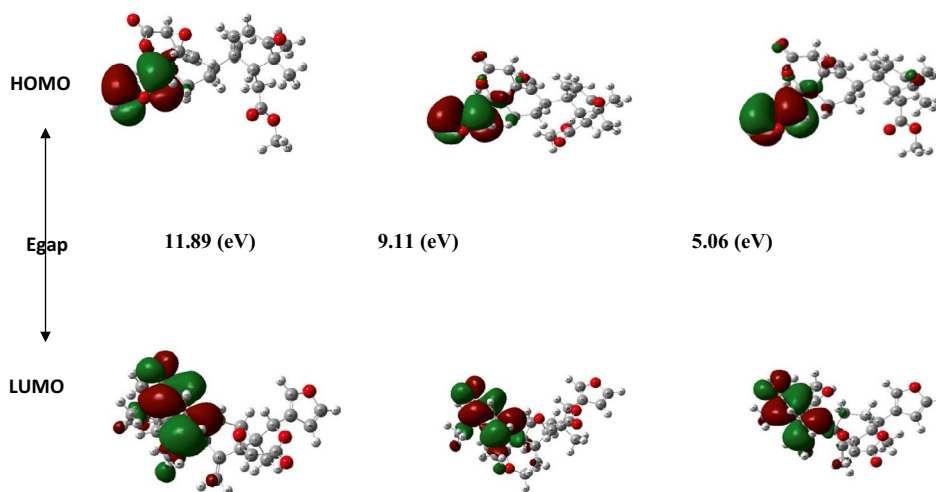
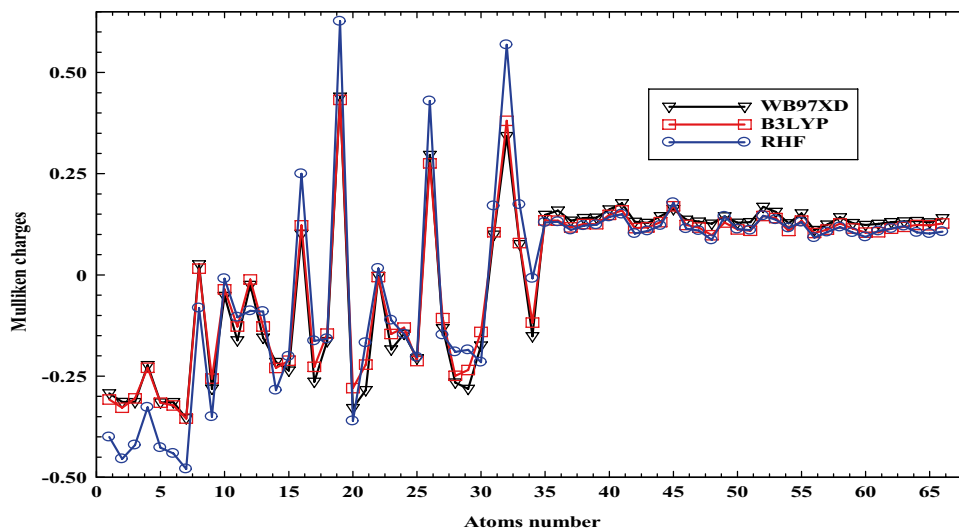
Fig. 10 HOMO and LUMO orbitals of andirobin for B3LYP, wB97XD and RHF methods**Fig. 11** Analysis of the atomic charge of andirobin

Table 6 Thermodynamic properties of andirobin at T=298.15 K and P=1 atm

Position	Energy (kcal mol ⁻¹)			Heat Capacity (Cal mol ⁻¹ K ⁻¹)			Entropy (kcal mol ⁻¹ K ⁻¹)		
	RHF	B3LYP	wB97XD	RHF	B3LYP	wB97XD	RHF	B3LYP	wB97XD
Translational	0.889	0.889	0.889	2.981	2.981	2.981	44.320	44.320	44.320
Rotational	0.889	0.889	0.889	2.981	2.981	2.981	37.075	37.095	36.873
Vibrational	385.695	361.275	365.948	110.805	120.569	117.926	113.149	122.310	117.349
Electronic	0.000	0.000	0.000	0.000	0.000	0.000	0.000	0.000	0.000
Total	387.473	363.052	367.725	116.767	126.530	123.888	194.545	203.724	198.542

Table 7 Values of the components α and β of andirobin calculated by RHF, B3LYP and wB97XD methods with 6–311 G(d,p) basis set

Setting	RHF	wB97XD	B3LYP
α_{xx} (au)	306.485464	322.779676	345.592110
α_{xy}	0.178284026	14.0958798	-1.25190072
α_{yy}	258.608305	263.537667	287.321112
α_{xz}	-15.6883622	-14.4220451	-16.6752659
α_{yz}	14.5654454	-3.83748276	14.2280413
α_{zz}	260.664368	289.907663	273.732329
$\alpha_0(10^{-23} esu)$	4.079	4.329	4.479
$\Delta\alpha(10^{-23} esu)$	0.886	0.926	1.130
μ_x	-1.45964701	-0.964075973	-1.22952899
μ_y	1.22302364	2.19030001	1.27947709
μ_z	-2.36548828	-1.30554236	-2.14712588
μ_{tot} (Debye)	7.719	6.929	7.080
β_{xxx} (au)	-152.766044	-186.527249	-164.746249
β_{xxy}	13.2011898	49.9667445	-42.7350655
β_{xyy}	-17.3049014	-36.2281147	-45.0707871
β_{yyy}	31.5960858	157.862321	41.5364778
β_{xxz}	-41.9751411	-12.0131608	-72.1860780
β_{xyz}	-9.03400418	22.5166009	-23.5196702
β_{yyz}	-61.3570970	-41.4362200	-92.5383749
β_{zzz}	-57.7683282	-98.0751745	-88.2534186
β_{yzz}	-0.892812011	6.07661894	-18.6288423
β_{zzz}	-145.794968	-139.306169	-151.764380
$\beta_0(10^{-33} esu)$	2941.205	3724.356	3759.876

(R1) O1–C8 means the bond length between atom 1 which is Oxygen and atom 8 which is Carbon as labelled on the diagram. (A1) C16, O2, C19 means the bond angle between C–O–C as labelled on the diagram

can be used for nonlinear optical applications. Therefore, our results obtained on the andirobin molecule indicate that this compound is a potential candidate for the emergence of the technology in many devices.

Acknowledgements We are thankful to the Council of Scientific and Industrial Research (CSIR), India for financial support through Emeritus Professor scheme (Grant No. 21(0582)/03/EMR-II) to Prof. A.N. Singh of the Physics Department, Bahamas Hindu University, India which enabled him to purchase the Gaussian Software. We are most

grateful to Emeritus Prof. A.N. Singh for donating this software to Prof Geh Wilson Ejuh, University of Dschang, IUT-FV Bandjoun, Cameroon.

Declarations

Conflict of interest The authors declare that they have no conflicts of interest.

Open Access This article is licensed under a Creative Commons Attribution 4.0 International License, which permits use, sharing, adaptation, distribution and reproduction in any medium or format, as long as you give appropriate credit to the original author(s) and the source, provide a link to the Creative Commons licence, and indicate if changes were made. The images or other third party material in this article are included in the article's Creative Commons licence, unless indicated otherwise in a credit line to the material. If material is not included in the article's Creative Commons licence and your intended use is not permitted by statutory regulation or exceeds the permitted use, you will need to obtain permission directly from the copyright holder. To view a copy of this licence, visit <http://creativecommons.org/licenses/by/4.0/>.

References

- Pope M, Swenberg CE (1984) Electronic processes in organic solids. *Ann Rev Phys Chem* 35:613–655
- Miyake T, Ishimoto S, Ishimatsu N, Higuchi K, Minoura K, Kikuchi T, Tanaka R (2015) Carapanolides T-X from *Carapa guianensis* (Andiroba) seeds. *Molecules* 20:20955–20966. <https://doi.org/10.3390/molecules201119737>
- Inoue T, Ohmori S, Kikuchi T, Yamada T, Tanaka R (2018) Carapanosins D-F from the seeds of andiroba (*Carapa guianensis*, Meliaceae) and their effects on LPS-activated NO production. *Molecules* 23(7):1778. <https://doi.org/10.3390/molecules23071778>
- Jittaniyom C, Sommit D, Muangsin N, Pudhom K (2012) Andirobin from *X moluccensis*. *Acta Cryst E* 68:o2550–o2551. <https://doi.org/10.1107/S1600536812027705>
- Ollis WD, Ward AD, De Oliveira MH, Zelnik R (1970) Andirobin. *Tetrahedron* 26(7):1637–1645. [https://doi.org/10.1016/S0040-4020\(01\)93014-5](https://doi.org/10.1016/S0040-4020(01)93014-5)
- De Toledo TA, da Silva LE, Botelho TC, Ramos RJ, de Souza PT, Teixeira AMR, Freire PTC, Bento RRF (2012) Characterization of flavonoid 3-Methoxyquercetin performed by FT-IR and FT-Raman spectroscopies and DFT calculations. *J Mol Struct.* <https://doi.org/10.1016/j.molstruc.2012.06.058>
- Melo IRS, Teixeira AMR, Sena DM, Santos HS, Albuquerque M, Bandeira PN, Rodrigues AS, BrazFilho R, Gusmao GOM, Silva JH, Faria JLB, Bento RRF (2014) FT-Raman and FTIR-ATR

- spectroscopies and DFT calculations of triterpene acetyl aleuritic acid. *J Mol Struct* 1058:221–227. <https://doi.org/10.1016/j.molstruc.2013.11.023>
8. Cheng Y-B, Chien Y-T, Lee J-C, Tseng C-K, Wang H-C, Lo I-W, Wu Y-H, Wang S-Y, Wu Y-C, Chang F-R (2014) Limonoids from the Seeds of *Swietenia macrophylla* with inhibitory activity against dengue virus 2. *J Nat Prod* 77:112367–112374. <https://doi.org/10.1021/np5002829>
 9. Sidjui LS, Nganso YOD, Toghueo RMK, Brussine NK, Wakeu BNK, Joel T, Dameue JT, Mkounga P, Adhikari A, Lateef M, Folefoc GN, Muhammad SA (2018) Kostchyienones A and B, new antiplasmodial and cytotoxicity of limonoids from the roots of *Pseudocedrela kotschyi* (Schweinf.) Harms Z. *Naturforsch.* 73(3–4):153–160. <https://doi.org/10.1515/znc-2017-0102>
 10. Frisch MJ, Trucks GW, Schlegel HB, Scuseria GE, Robb MA, Cheeseman JR, Scalmani G, Barone V, Mennucci B, Petersson GA, Nakatsuji H, Carito M, Li X, Hratchian HP, Izmaylov AF, Bloino J, Zheng G (2009) Gaussian 09, Revision A. 02. Gaussian, Inc., Wallingford CT
 11. Fonkem C, Ejuh GW, Tchangnwa NF, Yossa KR, Ndjaka JMB (2020) Theoretical study of optoelectronic properties of the molecule 2-cyano-3-[4-(diphenylamino) phenyl] acrylic acid. *J Iran Chem Soc* 17:533–543. <https://doi.org/10.1007/s13738-019-01790-4>
 12. Hossian MI, Kumer A, Begum SH (2018) Synthesis and characterization of ammonium benzoate and its derivative based ionic liquids and their antimicrobial Studies *Asian. J Phys Chem Sci* 3:1–9. <https://doi.org/10.9734/AJOPACS/2018/39148>
 13. Tchangnwa NF, Ejuh GW, Ndjaka JMB (2017) Theoretical study of optoelectronic and thermodynamic properties of molecule 4-[2-(2-N, N-dihydroxy amino thiophene)vinyl]benzamine: Influence of hydroxyl position. *Mater Lett* 202:89–95. <https://doi.org/10.1016/j.matlet.2017.05.064>
 14. Mveme CDD, Tchangnwa NF, Ejuh GW, Yossa Kamsi RA, Ndjaka JMB (2020) Frequency down-conversion of multiline CO laser into the THz range with ZnGeP2 crystal. *Opt Quantum Electron* 52:1
 15. Fankam JBF, Ejuh GW, Tchangnwa Nya F, Ndjaka JMB (2020) Study of electronic structure, optoelectronics, linear and non-linear optical properties and chemical descriptors of dibromodinitrofluorescein isomers in gas phase and solvent media using Ab Initio and DFT Methods. *Chin J Phys* 66:461–473. <https://doi.org/10.1016/j.cjph.2020.05.015>
 16. Yossa Kamsi RA, Ejuh GW, Mkounga P, Ndjaka JMB (2020) Study of the molecular structure, electronic and chemical properties of Rubescin D molecule. *Chin J Phys* 63:104–121. <https://doi.org/10.1016/j.cjph.2019.10.016>
 17. Yossa Kamsi RA, Ejuh GW, Tchhoffo F, Mkounga P, Ndjaka JMB (2019) Electronic structure, spectroscopic (IR, Raman, UV Vis, NMR), Optoelectronic, and NLO properties investigations of Rubescin E (C₃₁H₃₆O₇) molecule in gas phase and chloroform solution using Ab Initio and DFT Methods. *Adv Cond Matt Phys.* 2019:1–22. <https://doi.org/10.1155/2019/4246810>
 18. Jeyavijayan S (2015) Molecular structure, vibrational spectra, NBO analysis, first hyperpolarizability, and HOMO–LUMO studies of 2-amino-4-hydroxypyrimidine by density functional method. *J Mol Struct* 1085:137–146
 19. Zahra A, Mehdi DE, Esmail V, Manzarbanou A, Saeideh Y, Ali K (2017) A structural study of fentanyl by DFT calculations, NMR and IR spectroscopy. *J Mol Struct* 1128:552
 20. Rastogi VK, Palafox MA, Tanwar RP, Mittal L (2002) *Spectrochim. Acta A.* 58:403
 21. Silverstein RM, Basseler GC, Morill TC (1962) Spectrometric identification of organic compounds. *J Chem Edu* 39:546
 22. Bühl M, Kaupp M, Malkina OL, Malkin VG (1999) The DFT route to NMR chemical shifts. *Comput Chem* 20:91
 23. Perera SA, Nooijen M, Bartlett RJ (1996) Electron correlation effects on the theoretical calculation of nuclear magnetic resonance spin–spin coupling constants. *J Chem Phys* 104:3290
 24. Karabacak M, Kurt M, Cinar M, Coruh A (2009) Experimental (UV, NMR, IR and Raman) and theoretical spectroscopic properties of 2-chloro-6-methylaniline. *Mol Phys* 107:253
 25. Scrocco E, Tomasi J, Lowdin P (1978) *Advances in quantum chemistry.* Acad Press 11:115
 26. Chemla DS, Zyss J (1987) *Nonlinear Optical Properties of Organic Molecules and Crystals.* Academic Press, 1 Chap. 2, 18. ISBN 9780121706111, 9780323148153
 27. Tasal E, Kumalar M (2012) Ab initio Hartree–Fock and density functional theory investigations on the conformational stability, molecular structure and vibrational spectra of 5-chloro-3-(2-(4-methylpiperazin-1-yl)-2-oxoethyl)benzo[d]thiazol-2(3H)-one drug molecule. *Spectrochim Acta A Mol Biomol Spectrosc* 95:282. <https://doi.org/10.1016/j.saa.2012.04.081>
 28. Soscún H, Castellano O, Bermúdez Y, Toro-Mendoza C, Marcano A (2002) Linear and nonlinear optical properties of pyridine N-oxide molecule. *J Mol Struct* 592:19
 29. Thanthirawat KS, de Silva KN (2002) Non-linear optical properties of novel fluorenyl derivatives: ab initio quantum chemical calculations. *J Mol Struct* 617:169
 30. Karakas A, El Kouari Y, Migalska-Zalas A, Sahraoui B (2012) *Photon Lett Pol* 4(1):17–19
 31. Ortyl E, Chan SW, Nunzi JM, Kucharski S (2006) Second harmonic generation by all-optical poling and its relaxation in the polymer films containing azo sulfonamide chromophores. *Opt Mater* 29:268–272
 32. Andraud C, Brotin T, Garcia PF, Goldner P, Bigot B, Collet A (1994) Theoretical and experimental investigations of the nonlinear optical properties of vanillin, polyvanillin, and bisvanillin derivatives. *J Am Chem Soc* 116:2094–2102

Publisher's Note Springer Nature remains neutral with regard to jurisdictional claims in published maps and institutional affiliations.